Is Actin Filament and Microtubule Growth Reaction- or Diffusion-Limited?

Johannes Pausch[1], **Gunnar Pruessner**[2]

[1,2] Department of Mathematics, Imperial College London, UK

[1] correspondance: j.pausch15@imperial.ac.uk

Abstract. Inside cells of living organisms, actin filaments and microtubules self-assemble and dissemble dynamically by incorporating actin or tubulin from the cell plasma or releasing it into their tips' surroundings. Such reaction-diffusion systems can show diffusion- or reaction-limited behaviour. However, neither limit explains the experimental data: while the offset of the linear relation between growth speed and bulk tubulin density contradicts the diffusion limit, the surprisingly large variance of the growth speed rejects a pure reaction limit. In this article, we accommodate both limits and use a Doi-Peliti field-theory model to estimate how diffusive transport is perturbing the chemical reactions at the filament tip. Furthermore, a crossover bulk density is predicted at which the limiting process changes from chemical reactions to diffusive transport. In addition, we explain and estimate larger variances of the growth speed.

4 February 2019

1. Introduction

Microtubules and actin filaments are structures that polymerise by incorporating and releasing their diffusively moving building blocks, tubulin and actin. They are responsible for growth, shape, movement, and transport processes, among others, and can span the entire cell [1, 2, 3]. Their dynamics have been studied intensively theoretically‡ and experimentally§. However, many questions about their dynamics remain debated or completely unanswered. This includes: Is their growth limited by diffusion to their tip [10, 18] or by the chemical reaction rates for incorporation [9, 18]? How can the large variance of their growth be explained [14]?

In experiments, the filament growth speed $\langle v \rangle$ can be measured as a function of the bulk density ζ of tubulin or actin§. An effective incorporation coefficient k_{on} and effective release rate k_{off} are determined as parameters of a linear fit of growth speed data over bulk concentration ζ

$$\langle v \rangle = h(k_{\text{on}}\zeta - k_{\text{off}}), \tag{1}$$

where h is the effective growth length per incorporated particle. There are two mean field approaches for modeling the filament growth speed $\langle v \rangle$.

The first approach assumes that diffusive transport is quicker than the chemical reactions [4, 6, 7, 8, 9] and that polymerisation is therefore *reaction-limited*. This effectively infinite diffusivity D implies that particle concentration is homogeneous, and in particular, that there is no significant depletion close to the filament tip. Thus, filament growth is determined by two Poisson processes, incorporation with rate $\lambda\zeta$ and release with rate τ, each of which is associated with a step of length h. The two competing processes create a Skellam distribution [19] with expected growth speed $\langle v \rangle_R$ and effective diffusion constant D_{eff}

$$\langle v \rangle_R = h(\lambda\zeta - \tau) \quad \text{and} \quad D_{\text{eff}} = h^2(\lambda\zeta + \tau). \tag{2}$$

If the system is at the reaction limit, the effective and reaction limit's coefficients are equal, i.e. $k_{\text{on}} = \lambda$ and $k_{\text{off}} = \tau$. However, in comparison with experiments [14, 11, 16], D_{eff} is too small. Furthermore, it implies an independence of the growth speed from the viscosity of the medium, which was rejected experimentally for actin filaments [18] and microtubules [20]. Thus, a purely reaction-limited behaviour is rejected.

The second approach assumes that transport by diffusion is slower than the chemical reactions [18, 10] and that self-assembly is therefore *diffusion-limited*. The slow transport is not referring to position in $\mathbb{R}^3$ only, but in general includes orientation of the reactants in configuration space too [21]. This implies that, due to the incorporation into the tip, the building blocks are depleted locally. The growth speed is determined by the diffusive flux to the tip. If the protein concentration $c(x,t)$ follows a steady state

‡ Theoretical work includes [4, 5, 6, 7, 8, 9, 10] for microtubules and [5, 11, 12, 13] for actin filaments.
§ See Table S1 in the Supplemental Information of [14] for measured microtubule assembly rates. For actin filaments, assembly rates can be found in [15, 11, 16, 17]. In both cases, the rates are determined by measuring the filament growth speed $\langle v \rangle$ for several bulk densities ζ.

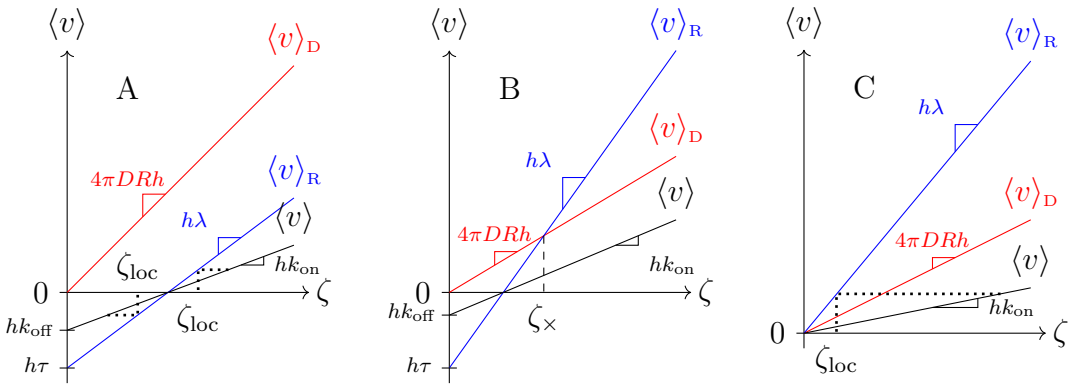

Figure 1. Filament growth speed $\langle v\rangle$ as function of the bulk density ζ of its building blocks. The diffusion-limited $\langle v\rangle_D$ (red), the reaction-limited $\langle v\rangle_R$ (blue), and the real growth speed $\langle v\rangle$ (black) are shown. A: The system is dominated by its reaction limit. B: Reaction-limited growth changes to diffusion-limited growth at the crossover bulk density $\zeta_\times$, C: The system is dominated by its diffusion limit. There is no release of building blocks from the tip, i.e. $k_{\text{off}} = 0$ and $\tau = 0$. Dotted lines in panels A and C: local densities at the tip ζ_{loc} can be read off as the bulk density at which reaction-limited growth leads to the same speed. This also holds in panel B, but is not depicted for better readability.

diffusion equation $0 = D\Delta c(x,t)$, the particle flux J through the absorbent reaction sphere of radius R and the growth length h determine the growth speed $\langle v\rangle_D$,

$$\langle v\rangle_D = Jh = 4\pi DRh\zeta, \tag{3}$$

which is equivalent to Smoluchowski coagulation [22] if the orientation of the reactants does not matter. If the orientation is important, then a smaller, effective reaction radius R leads to the same relation (3) [23]. If the system is at the diffusion limit, the effective incorporation coefficient equals the volume flux, i.e. $k_{\text{on}} = 4\pi DR$. However, this limit cannot accommodate a release rate k_{off} as any released particle would immediately be reabsorbed before diffusion can transport it away from the reaction surface. Furthermore, using this approach with typical parameters of microtubule assembly, only a small reduction of the bulk tubulin density to 89% is found at the reaction surface [10]. It therefore is not completely absorbent, as is theoretically suggested in [24]. According to the Stokes-Einstein equation [25] for small Reynolds numbers, diffusion-limited growth implies that viscosity and incorporation rate are inversely proportional [26] without offset. Tested in [18] and [20], small offsets for the growth of microtubules and the barbed actin filament ends are found, while a significant offset is found for the pointed ends of actin filaments. Thus, filament growth cannot be perfectly diffusion-limited either. Furthermore, this model is not probabilistic and therefore, it is not clear how to derive a variance of the growth speed.

Hence, experimental data suggests that microtubule and actin filament growth is neither perfectly reaction-, nor perfectly diffusion-limited. The objective of this article is to go beyond these two categories and understand their interplay better. The diffusion-

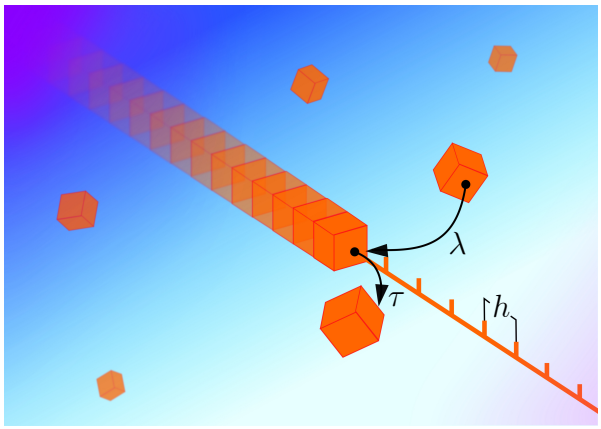

Figure 2. Schematic of the filament self-assembly process. Its building blocks move diffusively in $\mathbb{R}^3$. The filament tip is on a lattice with spacing h. Particles can be incorporated in the filament (coefficient λ) and released by it (rate τ).

(Eq. (3)) and reaction-limited (Eq. (2)), as well as the measured growth speed are schematically depicted in Fig. 1. Measured growth and shrinking speeds will always be slower than both limits for the following reasons. 1) When the filament is shrinking, the chemically possible, maximal shrinking speed is not attained because diffusion slows down transport away from the tip, leading to a locally higher particle density. 2) Analogously, when the filament is growing, the reaction-limited speed is not attained either because diffusion fails to maintain the bulk particle density around the tip. In both cases, the local density at the tip ζ_{loc} can be read off as the bulk density at which the reaction-limited speed is equal to the measured speed (dotted line). In principle, there are three cases: the reaction-limited case A, the mixed case B, where a crossover from reaction-limited to diffusion-limited behaviour occurs at the crossover bulk density $\zeta_\times$, and case C, where shrinking does not occur and the growth is limited by diffusion at all bulk particle densities.

2. Model

Theoretically, progress can be made by going beyond mean field theory which allows to calculate how chemical reactions are perturbed by diffusive transport of the reactants. Here, filament self-assembly is modelled on a three-dimensional lattice and described by a master equation (Appendix, Eq. (C28)). Following work by *Doi* [27] and *Peliti* [28], the probability generating function of this model can be found by transforming the model into a field theory. The derivation of the field theory is outlined briefly in Appendix B and Appendix C.

In our model, the building blocks and the filament tip are represented by fields, which are interpreted as time-dependent probability distributions of their positions. There is *no* field representing the filament as a whole, only its tip is modelled because it is the only part interacting with the building blocks. Due to the field representation,

they do not have a size. However, the finite size of the proteins is an important element of the step-wise filament growth. Therefore, our model is set up on a hybrid, three dimensional space: While particles move in continuous space $\mathbb{R}^3$, the filament tip is restricted to a discrete line $\mathbb{Z}$ with lattice constant h, overlaying the z-axis in $\mathbb{R}^3$, see Fig. 2. The persistence length P and flexural rigidity K of the filament we model are thus effectively infinite. This is a good approximation for microtubules ($P \approx 5200\mu m$, $K \approx 2 \cdot 10^{-23} Nm^2$), while for actin filaments, this approximation is slightly worse ($P \approx 18\mu m$, $K \approx 7 \cdot 10^{-26} Nm^2$) [29]. As we are modelling only a single polymer instead of the 13 microtubule protofilaments or the 2 actin filament strands, we interpret the lattice spacing h as the effective growth step length.

Each of the fields exists as an annihilation field and a creation field: $\varphi(x,t)$ and $\varphi^\dagger(x,t)$ for the building blocks, as well as $\psi_j(t)$ and $\psi_j^\dagger(t)$ for the filament tip. The creation field initiates a single particle or filament tip at the specified position and time, whereas the annihilation field measures their number at the point stated. Creation fields often appear as Doi-shifted fields [27], e.g. $\varphi^\dagger(x,t) = \widetilde{\varphi}(x,t) + 1\|$. In addition, the particle annihilation field is shifted to measure deviations from the bulk density ζ, i.e. $\varphi(x,t) = \check{\varphi}(x,t) + \zeta$. Between creation and annihilation, the system evolves by the stochastic processes included in the model.

There are six microscopic processes in our model. The units of the corresponding coefficients, denoted by $[\ldots]$, are written as monomials of T (time) and L (length). The last three microscopic processes are needed only for technical reasons and are eliminated at a later point.

- particle diffusion with constant D, $[D] = T^{-1}L^2$
- actin or tubulin absorption by the filament tip with coefficient λ and subsequent movement of the tip by distance h in the $+z$ direction, $[\lambda] = T^{-1}L^3$
- particle release from the filament tip with rate τ and subsequent movement of the tip by distance h in the $-z$ direction, $[\tau] = T^{-1}$
- actin/tubulin creation with coefficient γ, $[\gamma] = T^{-1}L^{-3}$
- extinction of actin/tubulin with rate r, $[r] = T^{-1}$
- extinction of the filament tip with rate ϵ, $[\epsilon] = T^{-1}$

The two extinction processes are included in the field theory for the technical reason of enforcing causality. After calculations, we take the limits $\gamma, r, \epsilon \to 0$ while keeping the ratio $\gamma/r = \zeta$ constant. Thus, the spontaneous extinction and creation are removed while a bulk density remains included.

All of the processes above are reflected in the action functional $\mathcal{A}$ of our model which splits up into a bilinear part and an interaction part $\mathcal{A} = \mathcal{A}_{\text{lin}} + \mathcal{A}_{\text{int}}$. The

‖ The field theory represents a systematic Taylor expansion of the probability generating function of the process. Without the Doi-shift, it is an expansion around 0, whereas with the Doi-shift, it is an expansion around 1. Details of the mapping between the field theory and the probability generating function can be found in [30]

diffusion and extinction of particles is represented in the particle bilinear part

$$\mathcal{A}_{\text{lin-P}} = \int_{\mathbb{R}^4} \widetilde{\varphi}(x,t)(-\partial_t + D\Delta - r)\check{\varphi}(x,t)\mathrm{d}^3x\mathrm{d}t, \tag{4}$$

where Δ is the spatial Laplace operator.

The filament tip is stationary without the processes of incorporation or release of tubulin. It is described by

$$\mathcal{A}_{\text{lin-F-stat}} = \int_{\mathbb{R}} \sum_{j\in\mathbb{Z}} \widetilde{\psi}_j(t)(-\partial_t - \epsilon)\psi_j(t)\mathrm{d}t. \tag{5}$$

However, due to incorporation and release, the bilinear part includes jumps in steps of 1_z

$$\mathcal{A}_{\text{lin-F-mov}} = \int_{\mathbb{R}} \sum_{j\in\mathbb{Z}} \Big(\overbrace{\lambda\zeta(\widetilde{\psi}_{j+1_z} - \widetilde{\psi}_j)\psi_j}^{\text{growing}} + \underbrace{\tau(\widetilde{\psi}_{j-1_z} - \widetilde{\psi}_j)\psi_j}_{\text{shrinking}} \Big)\,\mathrm{d}t, \tag{6}$$

where we omitted the time dependence of the fields for better readability. The first part corresponds to filament growth, while the second part describes shrinking of the filament. Jumps on the lattice are indicated by $\pm 1_z$.

All three bilinear actions together make up $\mathcal{A}_{\text{lin}} = \mathcal{A}_{\text{lin-P}} + \mathcal{A}_{\text{lin-F-stat}} + \mathcal{A}_{\text{lin-F-mov}}$.

The interaction part of $\mathcal{A}$ has the form

$$\begin{aligned}\mathcal{A}_{\text{int}} = \int_{\mathbb{R}} \sum_{j\in\mathbb{Z}} \Big[\lambda \Big(&\underbrace{(\widetilde{\psi}_{j+1_z} - \widetilde{\psi}_j)\psi_j\check{\varphi}(hj)}_{(a)} - \underbrace{\widetilde{\psi}_j\psi_j\widetilde{\varphi}(hj)\check{\varphi}(hj)}_{(b)} - \underbrace{\psi_j\widetilde{\varphi}(hj)\check{\varphi}(hj)}_{(c)} \Big) \\ &+ \underbrace{(\tau\widetilde{\psi}_{j-1_z} - \lambda\zeta\widetilde{\psi}_j)\psi_j\widetilde{\varphi}(hj)}_{(d)} + \underbrace{(\tau - \lambda\zeta)\widetilde{\varphi}(hj)\psi_j}_{(e)} \Big]\mathrm{d}t,\end{aligned} \tag{7}$$

where the time dependency is omitted for better readability.

The different parts of the interaction describe the following processes:

(a) the filament grows, i.e. the filament tip moves one step in the positive z direction upon incorporating an actin/tubulin particle;

(b) as particles are incorporated into the tip, its density is reduced locally, resulting in anticorrelations of the tip and the particle density;

(c) particle density is reduced by incorporation into the tip;

(d) in the presence of a tip, the particle density is increased by spontaneous release (τ) and decreased by incorporation ($\lambda\zeta$), leading to corresponding correlations of tip and particle densities;

(e) τ: particle density is increased because the filament releases a particle; $\lambda\zeta$: particle density is decreased because the filament incorporates a particle.

Field-theoretic propagations and interactions are schematically represented by Feynman diagrams. Particle propagation is drawn as a straight red line, filament

propagation is depicted as a curly blue line, and interactions are illustrated as vertices, see Fig. 3.

The interplay between propagation and interaction in a system governed by the action $\mathcal{A}$ can be calculated using the path integral. The system may be initialised by placing a filament tip at position $hj_0 = 0$ at time $t_0 = 0$. Then, the system evolves and particle concentrations, the filament tip positions, or moments of their distributions can be measured at a later point in time. In general, if the observable that we want to measure is represented by a combination of fields $\mathcal{O}(t)$, then its time-dependent, spatial probability distribution is given by the following path integral (see e.g. [31] for a detailed review)

$$\langle \mathcal{O}(t)\psi_0^\dagger(0)\rangle := \sum_{\ell=0}^{\infty} \int \mathcal{D}[\varphi,\psi]\mathcal{O}(t)\psi_0^\dagger(0) e^{-\mathcal{A}_{\text{lin}}} \frac{(-\mathcal{A}_{\text{int}})^\ell}{\ell!}. \tag{8}$$

Formally, this integral is summing all variations of all fields involved of all stochastic processes possibly occurring. The path integral is normalised such that

$$\langle 1\rangle = \sum_{\ell=0}^{\infty} \int \mathcal{D}[\varphi,\psi] e^{-\mathcal{A}_{\text{prop}}} \frac{(-\mathcal{A}_{\text{int}})^\ell}{\ell!} = 1. \tag{9}$$

The ℓ-th term of the series is the contribution of all processes with ℓ interactions.¶ The distribution of the filament's tip position j is given by $\langle \psi_j(t)\psi_0^\dagger(0)\rangle$. The expected growth speed and its variance are then determined by calculating the filament's expected position and its variance after time t.

3. Results

In the following, we consider three approximations of $\langle \psi_j(t)\psi_0^\dagger(0)\rangle$: Firstly, $\langle \psi_j(t)\psi_0^\dagger(0)\rangle_0$ is the reaction-limited distribution, cutting the sum in Eq. (8) at $\ell = 0$, which results

¶ These interactions are in the field-theoretic sense. In fact, the term for $\ell = 0$ already includes an arbitrary number of chemical interactions.

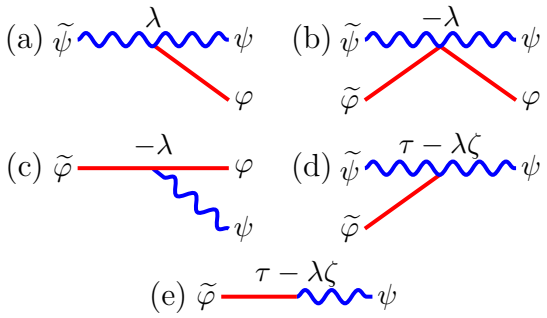

Figure 3. The stochastic processes that appear in $\mathcal{A}_{\text{int}}$, Eq. (7), are represented as amputated vertices in Feynman diagrams. Curly blue lines represent filaments, while straight red lines stand for their building blocks, actin or tubulin. In Doi-Peliti field theory, the convention is that all Feynman diagrams are read from right to left.

in only one Feynman diagram shown in Eq. (10). Secondly, $\langle\psi_j(t)\psi_0^\dagger(0)\rangle_2$ is terminating the sum at $\ell = 2$, resulting in two diagrams shown in Eq. (10) and (11). Thirdly, $\langle\psi_j(t)\psi_0^\dagger(0)\rangle_{\mathrm{Dy}}$ is the Dyson sum, which contains terms of all orders but selects only those Feynman diagrams whose loops are arranged daisy-chain-like, shown in Eq. (10) to Eq. (12):

$\langle\psi_j(t)\widetilde{\psi}_0(0)\rangle_{\mathrm{Dy}} \;\hat{=}$ (10)

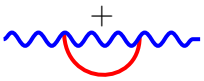

$+$ (11)

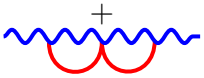

$+$ (12)

$+ \quad \ldots$

Not included in the Dyson sum approximation are terms whose Feynman diagrams have overlapping loops, e.g.

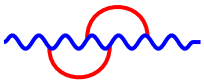 (13)

The physical interpretation of this approximation is as follows: repeated interactions between the filament tip and a building block are included, however, ignored are the cases where the repeated interactions of two building blocks with the filament overlap in time.

A priori, it is not clear which truncation of the path integral is a good approximation of the observable. However, a good agreement of the approximate result with experimental data indicates that the processes which were not included in the calculation rarely occur under experimental conditions.

The second and third approximation for the average filament growth speed are

$$\langle v\rangle_2 = h(\lambda\zeta-\tau)\Big(1-\underbrace{\lambda\Big(\frac{1}{4\pi DR}-\frac{h|\lambda\zeta-\tau|}{8\pi D^2}\Big)}_{\text{Loop correction term}}\Big), \tag{14}$$

$$\langle v\rangle_{\mathrm{Dy}} = \frac{h(\lambda\zeta-\tau)}{1+\lambda\Big(\frac{1}{4\pi DR}-\frac{h|\lambda\zeta-\tau|}{8\pi D^2}\Big)}. \tag{15}$$

The approximation $\langle v\rangle_0$ is given by $\langle v\rangle_2$ without the loop correction term. The derivation of Eq. (14) is outlined in Appendix E.

The loop correction term takes into account that, due to diffusive transport, the reaction-limited speed is reduced further because the locally depleted particles have to reach the effective reaction sphere of radius R. Considering the first term of the loop correction, if the diffusion is strong, the chemical reactions are less hindered by slow transport and the growth speed is closer to its reaction limit. This diffusion correction is itself corrected in the second term of the loop correction which describes how quickly the tip reaches regions that are less depleted. It predicts a non-linear dependence of

the growth speed $\langle v \rangle$ on the bulk particle density ζ, which so far has not been observed experimentally. Therefore, we assume $\frac{1}{4\pi DR} \gg \frac{h|\lambda\zeta-\tau|}{8\pi D^2}$ and ignore the latter in the following. Thus, given the diffusion-limited growth coefficient $4\pi DR$ and the observed k_{on} and k_{off}, Eq. (1), we can calculate the reaction-limited λ as well as the offset τ

$$\lambda = k_{\text{on}} \frac{4\pi DR}{4\pi DR - k_{\text{on}}} \quad \text{and} \quad \tau = k_{\text{off}} \frac{4\pi DR}{4\pi DR - k_{\text{on}}}, \tag{16}$$

which is equivalent to the results in [32] for general reaction-diffusion systems. It follows, that the observed growth coefficient k_{on} is smaller than the reaction- and the diffusion-limited growth coefficients, i.e. $\frac{k_{\text{on}}}{\lambda} < 1$ and $\frac{k_{\text{on}}}{4\pi DR} < 1$, as shown in Fig. 1.

Furthermore, there is a bulk particle density $\zeta_\times$ at which diffusion becomes the defining limitation in comparison to reaction (Fig. 1, B):

$$\zeta_\times = \frac{k_{\text{off}}}{2k_{\text{on}} - 4\pi DR}. \tag{17}$$

For $k_{\text{off}} = 0$, if $4\pi DR > 2k_{\text{on}}$, then growth is reaction-limited otherwise it is diffusion-limited.

One of the open questions for microtubule and actin filament growth is the origin of large fluctuations [14, 11]. In part, they can be explained as an overlap of the fluctuations of the reaction and diffusion processes. This is quantified by the effective diffusion constant (derived in Appendix F)

$$D_{\text{eff},2} = h^2(\lambda\zeta + \tau)\left(1 - \frac{\lambda}{4\pi DR}\right) + \lambda\frac{h|\lambda\zeta - \tau|}{2D\pi} \tag{18}$$

$$\approx h^2(k_{\text{on}}\zeta + k_{\text{off}}) + \lambda\frac{h|\lambda\zeta - \tau|}{2D\pi}, \tag{19}$$

which is larger than the reaction-limited effective diffusion in Eq. (2). The approximation in the last line, Eq. (19), is good only if the system is close to the reaction-limit, i.e. if $\lambda \ll 4\pi DR$. Eq. (19) includes a correction to Eq. (2): it incorporates additional fluctuations of the filament length caused by the diffusion of the building blocks in the vicinity of the filament tip. We use Eq. (19) for the following comparison with experimental data.

4. Comparison with Experimental Data

The experimental values of the parameters used above are not unique, as they depend on additional aspects of the experimental setup: Is the experiment *in vitro*, with control over microtubule-associated proteins (MAPs), or *in vivo*, where a variety of MAPs can influence the dynamics?, Which type of tubulin (e.g. GTP or GMPSPP[14]) was used?, Which polymerization buffers were used for actin?, Are the filaments fixed and only one end has to be considered for growth, or is it free and can grow or shrink at both ends simultaneously?, Microtubule and actin filaments are polarized. Which end is measured?, Which method was used to determine the growth speed variation?, How was the measurement noise taken into account?

For the following experimental validation of our model, we

Reference		k_{on} $\mu M^{-1}s^{-1}$	k_{off} s^{-1}	ζ μM	$D_{\text{eff-m}}$ nm^2s^{-1}	D_{eff} (Eq. (2)) nm^2s^{-1}	R nm
Fujiwara et al. [11]	*Ca*	6.1	0.85	0.14	366	12.4	0.02
	Mg	10	0.64	0.06	421	9.3	0.03
Kuhn, Pollard [16]	*Mg*	7.4	0.8	0.16	226	14.5	0.02
Gardner et al. [14]	GMPCPP	5.1	3.9	1.5	28.8	4.2	0.13
	GTP	$1.5^{\star}$	$0.5^{\star}$	7.0	111	4	0.04
	GTP	$4.8^{\dagger}$	$15^{\dagger}$	7.0	111	17.5	0.13

Table 1. Experimental results for the incorporation rates k_{on} and release rates k_{off}: above dashed line: actin filament data, below dashed line: microtubule data. The theoretical value of the effective diffusion constant D_{eff} according to Eq. (2) depends on the specific bulk density ζ chosen in the experiment. Given the independently measured coefficients k_{on} and k_{off}, the expected effective diffusion constant is D_{eff} – using the uncorrected reaction-limited approach, Eq. (2); however, measured were diffusion constants $D_{\text{eff-m}}$. The two lines about the data from Fujiwara et al. [11] concern actin(Ca) and actin(Mg). GTP and GMPCPP refer to different types of tubulin. The data marked by * is taken from Fig. 6C in [14] and is significantly lower than typically measured values, which are marked by † and taken from table S1 in [14]. In all experiments, the expected effective diffusion coefficient D_{eff} is smaller than the measured one $D_{\text{eff-m}}$. The last column shows the effective interaction radius determined from Eqs. (16) and (19)

(i) use experimental data for the effective incorporation coefficient k_{on}, effective release rate k_{off}, and effective diffusion constant (denoted by $D_{\text{eff-m}}$) at a specified bulk density ζ from references [11, 16, 14],

(ii) calculate effective diffusion constant D_{eff} that is expected in the reaction limit (setting $k_{\text{on}} = \lambda$, $k_{\text{off}} = \tau$) using Eq. (2) and compare it to the actually measured constant $D_{\text{eff-m}}$

(iii) set the effective diffusion constant from our model, Eq. (19), to the measured one $D_{\text{eff-m}}$

(iv) infer the effective interaction radius R from our model using Eqs. (16) and (19) and compare it two estimates of R based on [26] and [21]

The experimental data and the calculated D_{eff} and R are shown in Table 1. Evaluating Eqs. (16) and (19), the bulk diffusion constant D of individual individual building blocks is chosen to be $D = 5 \cdot 10^7 nm^2 s^{-1}$ for actin in water [33, 34, 35], and $D = 5.9 \cdot 10^6 nm^2 s^{-1}$ for tubulin in sea urchin cytoplasm [36]. As tubulin has a length of $8nm$ and there are typically 13 protofilaments in a microtubule [37], the effective growth step size h is $0.6nm$ for the purpose of our calculations. Actin filaments consist of only two strands and the actin monomer length is approximately $7nm$ [38], however the monomers are not aligned in the filament, hence, an effective growth step size h of about $2.7nm$ is used [11].

Table 1 shows that for several experiments with actin filaments and microtubules,

the expected effective diffusion constant D_{eff} from Eq. (2) is smaller than the measured one, $D_{\text{eff-m}}$. One possible explanation for this higher variability of the growth length is that the polymerization steps occur in trimers or even larger groups of monomers ([11] for actin filaments, [39] for microtubles). However, more recent experiments challenge this explanation ([16] for actin filaments, [40] for microtubules).

Our model accommodates the measured effective diffusion constants D_{eff} without introducing such oligomer incorporation by choosing a suitable value of the effective reaction radius R. The values required (see Table 1) range from $R \approx 0.1nm$ to $R \approx 0.01nm$.

For comparison, we use the theoretical result in [26]: when two spheres whose sum of radii is R, and whose circular reaction interface has opening angle θ react in a diffusive environment, then the effective reaction radius is $R\sin(\theta/2)$ (Eq. (5) in [26]). When the reaction interface is small compared to the size of the particle, the effective reaction radius is equal to the diameter of the interface. In [21], the interface size for typical proteins (including actin monomers and tubulin) is estimated to be about $0.2nm$.

While our estimates are smaller but around the same order of magnitude, the discrepancy still asks for an explanation. Aside from the simplifications of the filament structure and behaviour made to obtain our model, in deriving the effective diffusion constant, it was assumed that a one-loop correction is sufficient, Eq. (19). While this one-loop correction does account for a larger effective diffusion constant, higher order corrections might be necessary to achieve a better agreement with the experimental data, in particular when the system is far away from the reaction limit. That our estimate of R is within a reasonable range suggests that our model suffices to capture the basic higher order interactions.

5. Conclusion

In conclusion, we found that in real systems with reaction and diffusion processes, there always is a superposition of their stochastic behaviour. This superposition will likely influence all observables, of which in this article we picked two: steady state filament growth speed $\langle v \rangle$ and its effective diffusion D_{eff}, quantifying the growth length variance.

We used a field theoretic model to calculate how the reaction limit of microtubule and actin filament growth is undermined due to imperfect diffusive supply of tubulin or actin, Eq. (15). The chemical reaction rates were deduced from the measured effective rates, the diffusivity and the effective reaction radius, Eq. (16). While the superposition of reactions and diffusion reduces the growth speed, it increases its fluctuations, Eq. (19). Therefore, we provide a partial explanation for the experimentally observed, large fluctuations in filament growth speed, Table 1. For the comparison, we assumed that the system is close to the reaction limit. Although our estimate of the reaction radius is somewhat smaller than expected, it has the correct magnitude, which suggests that the basic model is justified but may require further refinement. Other processes, such as hydrolysis in the filament cap, are also likely to contribute the anomalous fluctuations.

While our model captures stochastic aspects of reaction-diffusion systems accurately, it drastically simplifies the real filaments. Among other aspects, the model neither includes the cylinder structure of microtubules with its thirteen protofilaments, nor does it model the strand structure of actin filaments. In addition, hydrolysis in the cap of the filaments is ignored. Despite these simplifications, our model advances the understanding of the stochasticity of the real self-assembly by using an idealized filament. Expanding our model by replacing some idealization with more realistic features is left for future research.

Given the overlap of fluctuations due to chemical reactions and diffusive transport, it is likely for the filament growth speed to exhibit correlations in time, the study of which would be compelling for future research.

Acknowledgement

The authors thank Robert Endres, Guillaume Salbreux and Thomas Surrey for very helpful discussions. J.P. was supported by an EPSRC scholarship.

Appendix A. Conventions

In the following sections, many details of the calculations whose results are shown in the main text are presented. The field-theoretic calculations use the following conventions for the Fourier transformations:

$$\varphi(\omega,k) := \mathcal{F}[\varphi(t,x)](\omega,k) = \int_{\mathbb{R}^4} \varphi(t,x) e^{i\omega t - ikx} \mathrm{d}^3x \mathrm{d}t, \tag{A20}$$

$$\mathcal{F}^{-1}[\varphi(\omega,k)](t,x) = \int_{\mathbb{R}^4} \varphi(\omega,k) e^{-i\omega t + ikx} \text{đ}^3k \text{đ}\omega, \tag{A21}$$

$$\psi(\omega,k) := \mathcal{F}[\psi_j(t)](\omega,k) = \int_{\mathbb{R}} \sum_{j\in\mathbb{Z}^3} \psi_j(t) e^{i\omega t - ikhj} \mathrm{d}t, \tag{A22}$$

$$\mathcal{F}^{-1}[\psi(\omega,k)](\omega,k) = h^3 \int_{\mathbb{R}} \int_{[0,\frac{2\pi}{h}]^3} \psi(\omega,k) e^{-i\omega t + ikhj} \text{đ}^3k \text{đ}\omega, \tag{A23}$$

with $\text{đ}\omega = \mathrm{d}\omega/(2\pi)$ and $\text{đ}^3k = \mathrm{d}^3k/(2\pi)^3$. Also used are the shorthands $\delta(\omega-\omega') = 2\pi\delta(\omega-\omega')$, $\delta^3(k-k') = (2\pi)^3\delta^3(k-k')$ and $\delta_c^3(k-k') = \sum_{j\in\mathbb{Z}^3}\delta^3(k-k'+j2\pi/h)$, where $\delta(\cdot)$ is the Dirac δ-function in one dimension and $\delta^3(\cdot)$ in three dimensions. Furthermore, $\Theta(t)$ denotes the Heaviside function.

Appendix B. Master equation

In order to model filament growth as a field theory, we follow the approach by *Doi* [27] and *Peliti* [28]. Our model for filament growth is described by a master equation. It includes six processes:

(1) diffusion of actin or tubulin particles (diffusion constant D),

(2) tubulin or actin absorption by the filament tip (incorporation constant λ) and subsequent movement of the tip in z direction by one step on the lattice,

(3) tubulin or actin release (rate τ) and subsequent movement of the tip in $-z$ direction by one step on the lattice,

(4) creation of tubulin or actin (constant γ),

(5) extinction of tubulin or actin (rate r),

(6) extinction of the filament tip (rate ϵ).

The master equation describes in continuous time and on a discrete spatial lattice $h\mathbb{Z}^3$ how many microtubule or actin filament tips ($m_j \in \mathbb{N}_0$) and how many tubulin or actin particles ($n_j \in \mathbb{N}_0$) are at position $j \in \mathbb{Z}^3$. Let $\{m\}$ denote the entire filament tip occupation configuration in $h\mathbb{Z}^3$, and $\{n\}$ denote the respective tubulin/actin population. Then, we denote by $\mathcal{P}(\{m\},\{n\},t)$ the probability for the system to be in this configurations at time t. Furthermore, we use the shorthand 1_j for occupation of one filament tip / particle at position j, and we use the shorthand e_z for a unit step on the lattice in z direction. The master equation is:

$$
\begin{aligned}
\partial_t \mathcal{P}(\{m\},\{n\},t) = \sum_{j\in\mathbb{Z}^3}\Big[& && \text{(B24)}\\
(1)\qquad & D\sum_{|i-j|=1}\Big((n_j+1)\mathcal{P}(\{m\},\{n+1_j-1_i\},t) - n_j\mathcal{P}(\{m\},\{n\},t)\Big)\\
(2)\qquad & +\lambda\Big((m_j+1)(n_j+1)\mathcal{P}(\{m+1_j-1_{j+e_z}\},\{n+1_j\},t)\\
& -m_jn_j\mathcal{P}(\{m\},\{n\},t)\Big)\\
(3)\qquad & +\tau\Big((m_j+1)\mathcal{P}(\{m_j+1_j-1_{j-e_z}\},\{n-1_j\},t)\\
& -m_j\mathcal{P}(\{m\},\{n\},t)\Big)\\
(4)\qquad & +\gamma\Big(\mathcal{P}(\{m\},\{n-1_j\},t)-\mathcal{P}(\{m\},\{n\},t)\Big)\\
(5)\qquad & +r\Big((n_j+1)\mathcal{P}(\{m\},\{n+1_j\},t)-n_j\mathcal{P}(\{m\},\{n\},t)\Big)\\
(6)\qquad & +\epsilon\Big((m_j+1)\mathcal{P}(\{m+1_j\},\{n\},t)-m_j\mathcal{P}(\{m\},\{n\},t)\Big)\Big].
\end{aligned}
$$

Appendix C. Second Quantized Model

As outlined by *Doi* [27], the classical many particle equation (B24) can be transformed into a second quantized version. For this, time-independent occupation states $|\{m\},\{n\}\rangle$ are introduced, which represent the particle configuration, i.e. they tell us where how many filament tips ($\{m\}$) and tubulin or actin particles ($\{n\}$) are found. Furthermore, ladder operators a_j, $a_j^\dagger$ for filament tips and b_j, $b_j^\dagger$ for tubulin or actin are introduced. Their commutation rules are $[a_j, a_i^\dagger] = [b_j, b_i^\dagger] = \delta_{ij}$. All other commutators are zero.

Their action on occupation states is defined as

$$a_j|\{m\},\{n\}\rangle = m_j|\{m-1_j\},\{n\}\rangle, \tag{C25}$$
$$a_j^\dagger|\{m\},\{n\}\rangle = |\{m+1_j\},\{n\}\rangle, \tag{C26}$$
$$b_j|\{m\},\{n\}\rangle = n_j|\{m\},\{n-1_j\}\rangle, \tag{C27}$$
$$b_j^\dagger|\{m\},\{n\}\rangle = |\{m\},\{n+1_j\}\rangle. \tag{C28}$$

The state of the system is defined as

$$|\phi(t)\rangle = \sum_{\{m\},\{n\}} \mathcal{P}(\{m\},\{n\},t)|\{m\},\{n\}\rangle. \tag{C29}$$

Using Eq. (B24), the time derivative of $|\phi(t)\rangle$ can be written as

$$\begin{aligned}\partial_t|\phi(t)\rangle = \sum_{j\in\mathbb{Z}^3}\Big[&D\sum_{|i-j|=1}\Big(b_i^\dagger b_j - b_j^\dagger b_j\Big)\\ &+\lambda\Big(a_{j+e_z}^\dagger a_j b_j - a_j^\dagger a_j b_j^\dagger b_j\Big)+\tau\Big(a_{j-e_z}^\dagger a_j b_j - a_j^\dagger a_j\Big)\\ &+\gamma\Big(b_j^\dagger - 1\Big)+r\Big(b_j - b_j^\dagger b_j\Big)+\epsilon\Big(a_j - a_j^\dagger a_j\Big)\Big]|\phi(t)\rangle.\end{aligned} \tag{C30}$$

As described by *Peliti* [28], the second quantized state equation (C30) can be transformed into a field theory in path integral formulation. The result is presented in the main text of the article, Eqs. (4), (5), (6), and (7).

Appendix D. Propagators

In order to calculate moments of observables, the action in Eqs. (4), (5), (6), and (7) is Fourier transformed, using the convention from Eq. (A20). In Fourier-space, the propagators from Eqs. (4), (5), (6) are represented by lines in Feynman diagrams:

$$\hat{=}\quad \frac{\delta(\omega+\omega_0)\delta^3(k+k_0)}{-i\omega+Dk^2+r}, \tag{D31}$$

$$\hat{=}\quad \frac{\delta(\omega+\omega_0)\delta_c^3(k+k_0)}{-i\omega+\lambda\zeta(1-e^{-ihk_z})+\tau(1-e^{ihk_z})+\epsilon}, \tag{D32}$$

where incoming frequencies and momenta carry the subscript 0, while outgoing frequencies and moment do not have a subscript.

As the observables are probability distributions, after the Fourier transformation, the observables becomes their moment generating functions. Thus, moments and variances can be calculated as derivatives of the moment generating functions, evaluated at zero. This connection is used to calculated the expected filament growth speed and variance in the following sections.

Appendix E. Expected microtubule growth length

In a first approximation, truncating the sum in Eq. (8) at $\ell = 0$, we calculate the expected filament tip position without any loop corrections:

$$\langle hj_z\rangle_0 = i\partial_{k_z}\int_{\mathbb{R}}\langle\psi(\omega,k)\widetilde{\psi}(\omega',k')\rangle_0 \text{đ}\omega\Big|_{k_z=0} \tag{E33}$$

$$= i\partial_{k_z}\int_{\mathbb{R}}\frac{e^{-i\omega t}\text{đ}\omega}{-i\omega+\lambda\zeta(1-e^{-ihk_z})+\tau(1-e^{ihk_z})+\epsilon}\Big|_{k_z=0} \tag{E34}$$

$$= h(\lambda\zeta-\tau)te^{-\epsilon t}\Theta(t). \tag{E35}$$

If we now let the creation and extinction coefficients tend to zero while keeping their ratio $\zeta = \gamma/r$ constant, we find

$$\lim_{\epsilon\to 0}\langle hj_z\rangle_0 = h(\lambda\zeta-\tau)t\Theta(t). \tag{E36}$$

Hence, in this approximation, the filament growth speed is $\langle v\rangle_0 = \langle hj\rangle_0/t = h(\lambda\zeta-\tau)$, which is the reaction-limited growth speed, shown in Eq. (2) in the main article.

For the first correction $\langle v\rangle_2$, the process which is represented by the one-loop Feynman diagram, Eq. (11), has to be considered also:

$$\langle hj_z\rangle_2 = \langle hj_z\rangle_0 + i\partial_{k_z}\int_{\mathbb{R}^5}\langle\psi(\omega,k)\widetilde{\psi}(\omega',k')\rangle_2 \text{đ}\omega\text{đ}\omega_b\text{đ}k_b\Big|_{k_z=0} \tag{E37}$$

$$= \langle hj_z\rangle_0 + i\partial_{k_z}\int_{\mathbb{R}^5}\frac{\lambda(e^{-ihk_z}-1)(\tau e^{ihk_z}-\lambda\zeta)e^{-i\omega t}}{(-i\omega+\lambda\zeta(1-e^{-ihk_z})+\tau(1-e^{ihk_z})+\epsilon)^2} \tag{E38}$$

$$\frac{\text{đ}^3k_b\text{đ}\omega\text{đ}\omega_b}{(i(\omega_b-\omega)+\lambda\zeta(1-e^{-ih(k-k_b)_z})+\tau(1-e^{ih(k-k_b)_z})+\epsilon)(-i\omega_b+Dk_b^2+r)}\Big|_{k_z=0}$$

$$\approx \langle hj_z\rangle_0 + -h(\lambda\zeta-\tau)t\underbrace{\lambda\Big(\frac{\Lambda}{2\pi^2D}-\frac{h|\lambda\zeta-\tau|}{8\pi D^2}\Big)}_{\text{Loop correction term}}\Theta(t), \tag{E39}$$

where ω_b and k_b are the loop's free frequency and momentum:

$$\text{Loop}(\omega,k) = \int_{\mathbb{R}^4}\frac{\text{đ}^3k_b\text{đ}\omega_b}{(i(\omega_b-\omega)+\lambda\zeta(1-e^{-ih(k-k_b)_z})+\tau(1-e^{ih(k-k_b)_z})+\epsilon)(-i\omega_b+Dk_b^2+r)}$$

Here, we approximated $(1-e^{\pm ih(k_b-k)_z})$ by $\mp ih(k_b-k)_z$, as well as $(1-e^{\pm ihk_z})$ by $\mp ihk_z$. Then, a new variable $\tilde{k}_b$ is introduced, for which the z-component is shifted by $ih(\lambda\zeta-\tau)/(2D) = k_{b_z}-\tilde{k}_{b_z}$. Furthermore, we let r,ϵ tend to zero and we introduced a cutoff for the $\tilde{k}_b$ integral such that $|\tilde{k}_b|<\Lambda$. This cutoff Λ is identified as $\Lambda = \pi/(2R)$, where R is the effective radius of the reaction sphere.

Then, the calculation splits into a steady state part (shown here) and a relaxation part, where the latter tends to zero for large times t. Here, we focus on steady state solutions and omit the relaxation part. The average expected first correction to the growth speed is $\langle v\rangle_2 = \langle hj_z\rangle_2/t$, see Eq. (14) of the main article. Both corrections are graphically represented by Feynman diagrams in Eq. (10) and (11) of the main article.

The Dyson sum is a geometric sum over loop corrections where all the loops are daisy-chain-like, see Eq. (10) for the first three diagrams in the series. The associated expected position is

$$\langle hj_z\rangle_{\mathrm{Dy}} = \langle hj_z\rangle_0 + i\partial_{k_z}\int_{\mathbb{R}^5} \frac{\lambda(e^{-ihk_z}-1)(\tau e^{ihk_z}-\lambda\zeta)e^{-i\omega t}}{(-i\omega+\lambda\zeta(1-e^{-ihk_z})+\tau(1-e^{ihk_z})+\epsilon)^2} \tag{E40}$$

$$\cdot \frac{\mathrm{Loop}(\omega,k)}{1-\lambda\mathrm{Loop}(\omega,k)}\text{đ}\omega\Big|_{k_z=0}$$

$$\approx \frac{h(\lambda\zeta-\tau)t}{1+\lambda\left(\frac{\Lambda}{2\pi^2 D}-\frac{h|\lambda\zeta-\tau|}{8\pi D^2}\right)} \tag{E41}$$

where $\mathrm{Loop}(\omega,k)$ is the loop integral, i.e. the ω_b and $\tilde{k}_b$ integral over the second line of Eq. (E38). The speed is identified as $\langle v\rangle_{\mathrm{Dy}} = \langle hj_z\rangle_{\mathrm{Dy}}/t$.

Appendix F. Variance of microtubule growth length

First, we calculate the mean square displacement of the filament growth in the approximation without loops, i.e. the sum in Eq. (8) is truncated at $\ell = 0$:

$$\langle (hj_z)^2\rangle_0 = -\partial_{k_z}^2\int_{\mathbb{R}}\langle\psi(\omega,k)\widetilde{\psi}(\omega',k')\rangle_0\text{đ}\omega\Big|_{k_z=0} \tag{F42}$$

$$= h^2\Theta(t)e^{-\epsilon t}\Big((\lambda\zeta+\tau)t+(\lambda\zeta-\tau)^2t^2\Big). \tag{F43}$$

The variance is equal to

$$\mathrm{Var}_0(hj_z) = \langle (hj_z)^2\rangle_0 - \langle hj_z\rangle_0^2 \tag{F44}$$

$$= h^2\Theta(t)(\lambda\zeta+\tau)t, \tag{F45}$$

where we took the limit $\epsilon\to 0$. Hence, the variance of the average speed $\langle v\rangle_0$ decreases as $1/t$.

$$\mathrm{Var}_0(v) = \frac{\mathrm{Var}_0(hj_z)}{t^2} = \frac{h^2(\lambda\zeta+\tau)}{t}. \tag{F46}$$

These results represent the reaction-limited behaviour. As the variance of the growth length is linear in time, an effective diffusion constant $D_{0,\mathrm{eff}} = h^2(\lambda\zeta+\tau)$ can be associated. This observable is often considered as a sign for the fluctuations of the growth process. However, it characterises the reaction-limited fluctuations. In order to estimate the influence of additional, diffusive fluctuations, at least the first loop correction has to be calculated:

$$\langle (hj_z)^2\rangle_2 = \langle (hj_z)^2\rangle_0 - \partial_{k_z}^2\int_{\mathbb{R}}\frac{\lambda(e^{-ihk_z}-1)(\tau e^{ihk_z}-\lambda\zeta)e^{-i\omega t}\mathrm{Loop}(\omega,k)\text{đ}\omega}{(-i\omega+\lambda\zeta(1-e^{-ihk_z})+\tau(1-e^{ihk_z})+\epsilon)^2}\Big|_{k_z=0}$$

$$\approx \langle (hj_z)^2\rangle_0 + \underbrace{\lambda\frac{h|\lambda\zeta-\tau|^2}{2D\pi}t}_{\text{anomalous term}} \tag{F47}$$

$$- \Theta(t) \left(h^2(\lambda\zeta + \tau)t + 2h^2(\lambda\zeta - \tau)^2 t^2 \right) \underbrace{\lambda \left(\frac{\Lambda}{2\pi^2 D} - \frac{h|\lambda\zeta - \tau|}{8\pi D^2} \right)}_{\text{Loop correction term}},$$

where the same approximation as for Eq. (E37) where used, and the extinction rates ϵ and r were set to zero. The extra 'anomalous term' describes the additional fluctuations that go beyond the mean field calculations, which are described by a Skellam distribution [19].

In order to calculate the variance, the expected growth length squared has to be subtracted. However, as we are only considering the first correction, we omit all terms in which the 'Loop correction term' appears in a higher than linear order and find the result shown in Eq. (19) of the main article.

References

[1] Boal D 2012 *Mechanics of the Cell* (Cambridge University Press)
[2] Howard J 2001 *Mechanics of Motor Proteins and the Cytoskeleton* (Sinauer Associates, Inc.)
[3] Kolomeisky A B 2015 *Motor Proteins and Molecular Motors* (CRC Press, Taylor & Francis Group)
[4] Mitchison T and Kirschner M 1984 *Nature* **312** 237–242
[5] Frieden C 1985 *Annu. Rev. Biophys. Bio.* **14** 189–210
[6] Carlier M F, Melki R, Pantaloni D, Hill T and Chen Y 1987 *Proc. Natl. Acad. Sci. Unit. States Am.* **84** 5257–5261
[7] der Chen Y and Hill T 1987 *Proc. Natl. Acad. Sci. Unit. States Am.* **84** 8419–8423
[8] Walker R, O'Brien E, Pryer N, Soboeiro M, Voter W, Erickson H and Slamon E 1988 *J. Cell Biol.* **107** 1437–1448
[9] Bayley P 1993 *Nature* **363** 309
[10] Odde D J 1997 *Biophys. J.* **73** 88–95
[11] Fujiwara I, Takahashi S, Tadakuma H, Funatsu T and Ishiwata S 2002 *Nat. Cell Biol.* **4** 666–673
[12] Lan Y and Papoaian G A 2008 *Biophys. J.* **94** 3839–3852
[13] Guo K, Shillcock J and Lipowsky R 2009 *J. Chem. Phys.* **131** 1–11
[14] Gardner M K, Charlebois B D, Jánosi I M, Howard J, Hunt A J and Odde D J 2011 *Cell* **146** 582–592
[15] Pollard T D 1984 *J. Cell Biol.* **99** 769–777
[16] Kuhn J R and Pollard T D 2005 *Biophys. J.* **88** 1387–1402
[17] Fujiwara I, Vavylonis D and Pollard T D 2007 *Proc. Natl. Acad. Sci. Unit. States Am.* **104** 8827–8832
[18] Drenkhahn D and Pollard T D 1986 *J. Biol. Chem.* **261** 12754–12758
[19] Skellam J G 1946 *J. Roy. Stat. Soc.* **109** 296
[20] Wieczorek M, Chaaban S and Brouhard G J 2013 *Cell. Mol. Bioeng.* **6** 383–392
[21] Northrup S H and Erickson H 1992 *Proc. Natl. Acad. Sci.* **89** 3338–3342
[22] v Smoluchowski M 1917 *Z. Phys. Chem.* **92** 129–168
[23] Berg O G 1985 *Biophys. J.* **47** 1–14
[24] Collins F C 1950 *J. Colloid Sci.* **5** 499–505
[25] Sutherland W 1905 *Phil. Mag.* **9** 781–785
[26] Berg O G and von Hippel P H 1985 *Ann. Rev. Biophys. Chem.* **14** 131–160
[27] Doi M 1976 *J. Phys. A: Math. Gen.* **9** 1465–1477
[28] Peliti L 1985 *J. Phys.-Paris* **46** 1469–1483
[29] Gittes F, Mickey B, Nettleton J and Howard J 1993 *J. Cell Biol.* **120** 923–934
[30] Lan Y 2006 *J. Chem. Phys.* **125**
[31] Täuber U C 2014 *Critical Dynamics* (Cambridge University Press)

[32] Noyes R M 1961 *Prog. React. Kinet.* **1** 129–160
[33] Tait J F and Frieden C 1982 *Biochemistry* **21**(15) 3666–3674
[34] Lanni F, Taylor D L and Ware B 1981 *Biophys. J.* **35** 351–364
[35] Mihashi K 1964 *Arch. Biochem. Biophys.* **107**(3) 441–448
[36] Salmon E, Saxton W, Leslie R, Karow M and McIntosh J 1984 *J. Cell Biol.* **99** 2157–2164
[37] Mandelkow E, Thomas J and Cohen C 1977 *Proc. Natl. Acad. Sci.* 3370–3374
[38] Egelman E H 1985 *J. Muscle Res. Cell. Motil.* **6** 129–151
[39] Kerssemakers J W, Munteanu E L, Laan L, Noetzel T L, Janson M E and Dogterom M 2006 *Nature* **442** 709–712
[40] Schek H T, Gardner M K, Cheng J, Odde D J and Junt A J 2007 *Curr. Biol.* **17** 1445–1455